10

Surface Acoustic Wave Motors and Actuators: Mechanism, Structure, Characteristic and Application

Shu-yi Zhang and Li-ping Cheng
Lab of Modern Acoustics, Institute of Acoustics, Nanjing University
Nanjing 210093,
China

1. Introduction

Ultrasonic motors, as one kind of actuators, have attracted a lot of attention since it was proposed more than 20 years ago. In such kind of motors, the sliders (for linear motors) or the rotors (for rotary motors) are driven by the frictional forces between the sliders (rotors) and the stators when ultrasonic waves are propagating on the stators. Since then, the ultrasonic motors have been developed and applied successfully in wide fields, such as mechanical, optic, electronic, and automatic, as well as aeronautic and astronautic industries and technologies because of their unique advantages over conventional electro-magnetic ones, such as high driving forces and torques, easy controllability, quiet operation, non-electromagnetic induction, etc. (Sashida & Kenjo, 1993; Ueha & Tomikawa, 1993). Besides, with the rapid development of micro-electro-mechanical system (MEMS), miniature ultrasonic motors were developed (Dong et al., 2000; Zhang et al., 2006). However, the direct contact between the sliders (rotors) and the stators restricts the velocity and working lifetime of the motors, then a new kind of non-contact motors were presented, where a fluid is introduced between the stator and slider. Thus, instead of the frictional force, acoustic streaming excited by the acoustic wave on the stator and propagating in the fluid is used for driving the slider or rotor to move (Nakamura et al., 1990; Yamayoshi & Hirose, 1992; Hu et al., 1995; Cheng et al., 2007).

On the basis of conventional ultrasonic motors, several studies on new types of ultrasonic motors (actuators) with the driving forces coming from surface acoustic waves (SAWs) were presented (Moroney et al., 1989; Kurosawa et al., 1994). For the SAW motors, the SAWs are excited by interdigital transducers (IDTs) deposited on surfaces of piezoelectric substrates or thin films, and the SAW energies are concentrated in the thin layers near the surfaces of the substrates (for Rayleigh waves) or in the thin films (for Lamb waves). In addition to the characteristics of conventional ultrasonic motors, the SAW motors have more advantages, such as the high operation frequency, high speed, high energy density around the surfaces, and higher output force/torque, etc. Meanwhile, since the SAWs are excited by IDTs, which can be fabricated with planar technologies of semiconductor industries, the new types of motors are suitable for miniaturizing and integrating with integrated circuits and MEMS devices, etc.

Source: Acoustic Waves, Book edited by: Don W. Dissanayake,
ISBN 978-953-307-111-4, pp. 466, September 2010, Sciyo, Croatia, downloaded from SCIYO.COM

To overcome the difficulties of the frictional drive and extend the applications of the motors, several kinds of non-contact SAW linear motors (actuators) were developed (Sano, et al., 1997), in which a fluid layer (or a drop) is introduced between the stator and slider (rotor) of the actuator. Then a SAW streaming excited by the IDT and propagating in the fluid covered on the surface of the stator, instead of the frictional force, is used to drive the slider (rotor), by which the required driving power of the actuators is reduced greatly and the lifetime can be extended (Shiokawa, et al. 1990; Takeuchi, et al., 1994; Gu, et al., 2008). The non-contact SAW actuators have been widely used in chemical and biochemical fields (Takeuchi et al., 2005).

In this chapter, the structures and characteristics of IDTs for exciting SAWs and the excited SAW modes on different substrates are introduced briefly. Then the structures of the stators and sliders (rotors), theories and characteristics of the conventional contact linear and rotary SAW motors are presented. In addition, the mechanisms, structures and characteristics of non-contact SAW actuators, as well as some applications of the motors (actuarors), are also described and discussed.

2. Generation and propagation mode of SAWs

2.1 Structure and characteristic of interdigital transducers

SAWs can be generated by many different types of transducers. Up to now, a most popular and effective type of the transducers is the interdigital transducer (IDT), which consists of two interlocking comb-shaped metallic electrode arrays. For the simplest structure, the metallic electrodes have the same length (aperture) and the same width $\lambda/4$ as that of the gap, where λ is the SAW wavelength, as shown in Fig.1(a). The IDT is deposited on a piezoelectric substrate by the photolithographic technology. When a RF voltage with the same frequency as that of the IDT is applied to the IDT, the electric field components change sign from gap to gap, so that a corresponding periodic mechanical strain field is produced through the piezoelectric effect of the substrate.

The IDT radiates acoustic waves in both forward and backward directions, but unidirectional radiation can be obtained with special interdigital arrays. The simplest one is to use two identical interdigital transducers separated by a distance $(n+1/4)\lambda$, where n is an integer; both transducers are driven from two generators having 90 degree phase difference between them, or by a single generator with a quarter-wavelength of electrical transmission line connecting both transducers. As a result, the generated waves traveling to the right from each transducer add up, while those traveling to the left cancel from each other. The unidirectionality increases the conversion efficiency of the transducer by 3 dB since waves radiate in only one direction instead of two directions, and the bandwidth is reduced by this operation. In addition, for undirectional transducers, the waves incident to the left transducer from the right are not as strongly reflected as from a bidirectional array (White, 1970).

For the substrates with a weak piezoelectric effect, if the nonlinear effect is neglected, the SAW vibration amplitude is approximately proportional to the electrode number N, but the bandwidth is inversely proportional to N of the IDT. Meanwhile, in order to obtain the SAW field with appropriate homogeneity, the length of the electrodes (aperture) of the IDTs should also be suitably enlarged if the size of the IDT has no limit.

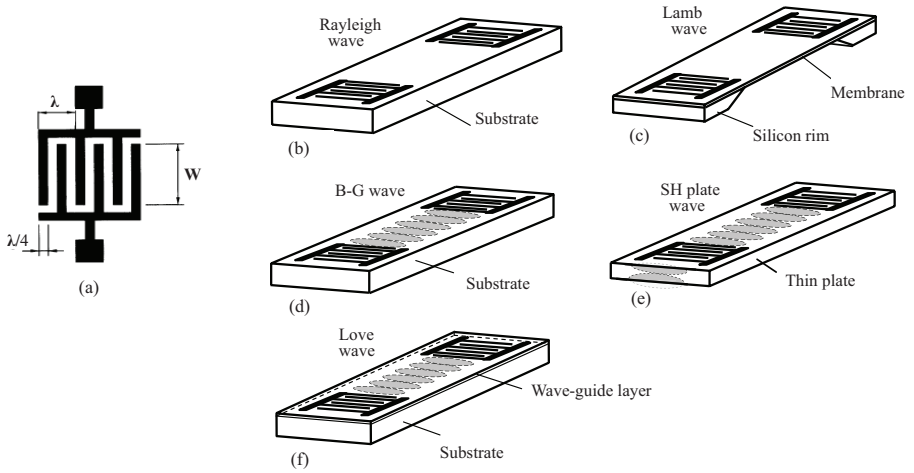

Fig. 1. Schematic diagram of transducer and SAW modes on different substrates: (a) interdigital transducer; (b) Rayleigh wave; (c) Lamb wave; (d) Bleustein-Gulyaev (B-G) wave; (e) shear horizontal plate wave; (f) Love wave

2.2 Mode and characteristic of SAWs

For different piezoelectric substrates, the IDT may excite waves with different modes, which depend on the materials and cut directions of the piezoelectric crystals or polarization directions of ceramics, as well as on the piezoelectric thin films with special growth directions on substrates. Generally, the wave modes are classified in five types as shown in Figs. 1(a)-1(f).

(i) In the Rayleigh wave mode shown in Fig.1(b), the surface particles in the sagittal plane of the substrate move in a retrograde elliptical trajectory relative to the SAW propagation direction, as shown in Fig.2(a). Besides, the amplitude of the Rayleigh mode decreases almost exponentially with the depth in the substrate, and the penetration depth of the wave is considered to be one wavelength range as shown in Fig.2(b). Therefore, the acoustic energy is concentrated in a thin layer beneath the surface with the depth about one wavelength of the Rayleigh wave. (ii) The Lamb wave propagates in a thin plate shown in Fig.1(c), so it is also called as the plate wave. There are two kinds of modes for Lamb wave, i.e., symmetric and anti-symmetric modes as shown in Fig.2(c), which may be considered as the composition of two Rayleigh waves propagating on both boundaries of a plate as the thickness of the plate is just over one wavelength. The symmetric and anti-symmetric modes of Lamb wave can be obtained by the composition of both Rayleigh modes with opposite phases and the same phases, respectively. (iii) For the Bleustein-Gulyaev (B-G) wave shown in Fig.1(d), it is a horizontally polarized surface wave propagating on an infinite piezoelectric substrate. (iv) For shear horizontal plate wave (SH plate wave) (see Fig.1(e)), the thickness of the substrate (thin plate) is half of the wavelength, and (v) for the Love wave (Fig.1(f)), the SH wave propagates in a thin layer covered on the substrate (White, 1970; Auld, 1973).

Therefore, for the last three kinds of the SAW modes, the vibrations of the surface particles are perpendicular to the wave propagation direction, but parallel to the surface of the

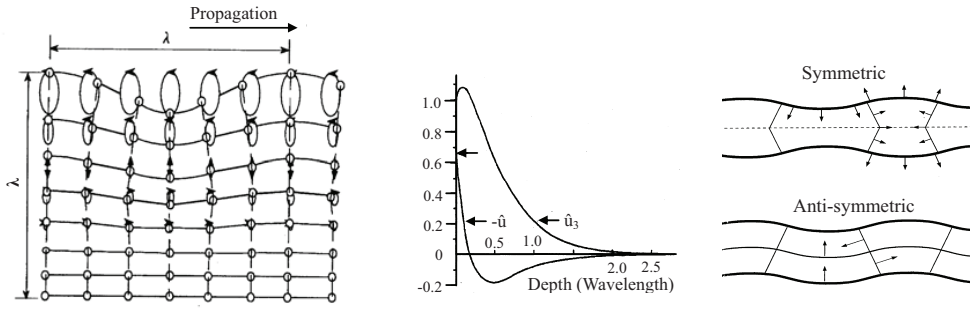

Fig. 2. Characteristics of SAWs propagating in elastic isotropic medium; (a) particle motion orbit of Rayleigh wave; (b) particle displacement of Rayleigh wave; (c) Lamb wave: symmetric and anti-symmetric modes.

substrate. For ultrasonic motors, the particle displacement of the surface is required to have a component perpendicular to the surface of the substrate, so, up to now, only Rayleigh and Lamb modes are used as the driving sources of the SAW motors.

3. Conventional SAW motors

Since a kind of ultrasonic micro-motors driven by Lamb waves with high frequencies excited by IDT was reported in 1989 (Moroney et al., 1989), several kinds of SAW motors driven by Rayleigh waves excited by IDTs have been developed. The first prototype of SAW linear motors was presented by Kurosawa et al., in which two pairs of IDTs with the central frequency about 10 MHz were prepared perpendicularly on a piezoelectric substrate, then two Rayleigh waves were excited in cross directions and a two-dimensional SAW motor was built-up (Kurosawa et al., 1994; 1996). Generally, for the conventional SAW linear motors, the sliders in contact with the stators are directly driven by the frictional forces between the sliders and stators. Based on the SAW linear motors, a kind of SAW rotary motor operated in similar conditions was also developed (Zhang et al., 2000). These SAW motors have similar operation principles, characteristics, and theories, which are described separately in this section.

3.1 Principle of SAW linear motors

SAW motors are composed of stators and sliders, where the stators are SAW devices (such as delay lines). A typical structure of SAW linear motors is shown in Fig.3(a) (Asai et al., 1999). The slider is in directly contact with the stator and driven by the frictional force between the slider and the stator induced by the SAW propagating in the stator. The acoustic wave mode used in the most of the conventional SAW motors is Rayleigh wave excited by IDT deposited on piezoelectric substrate. The driving force applied on the slider is induced by the particle motions and in the direction opposite to the SAW propagation. Since the amplitude of the Rayleigh wave decreases exponentially with the depth in the substrate, the acoustic energy is concentrated in a thin layer beneath the surface with a thickness of about one wavelength of the SAW. Therefore, the energy density is very high, which is beneficial for improving the utilization efficiency of the acoustic energy.

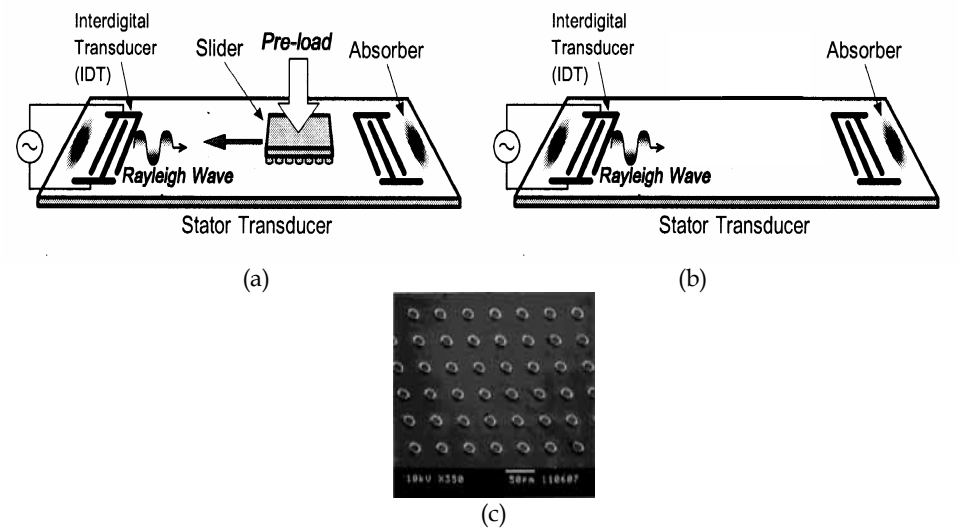

Fig. 3. SAW linear motor: (a) structure of motor; (b) stator with IDTs; (c) slider with projections on a Si wafer.

However, when the acoustic amplitude is large enough, the wave propagation may become nonlinear, such as generation of harmonic frequencies and frequency mixing. These effects may act as unwanted sources of wave attenuation. Therefore, in the practical applications of SAW motors, the operation conditions must be considered in compromise and optimization.

3.2 Structure of SAW linear motors

(a) SAW stators

For SAW motors, the ordinary SAW mode is Rayleigh waves, in which the substrates of 128^0 Y-cut X-propagation $LiNbO_3$ (128^0 YX-$LiNbO_3$) crystals are always used as the stators since the $LiNbO_3$ crystal substrates have a high electro-mechanical coupling coefficient, and the cut direction of $LiNbO_3$ crystals is the propagation direction of pure Rayleigh mode. Generally, one pair of IDTs are fabricated by the photolithographic technology on substrates as shown in Fig.3(b). One of the IDTs is applied by a RF voltage with the frequency consistent with the central frequency of the IDT, thus the SAW in Rayleigh mode is excited and propagating in two directions on the surface of the $LiNbO_3$ substrate. The other IDT can be used to receive the SAW for checking the wave propagation. In addition, some soft materials (absorbers) are applied on the areas between the IDTs and boundaries of the substrate to absorb the superfluous SAWs for eliminating the reflections of the boundaries. In the SAW motor studies, the SAW frequency is generally taken in the range of 1-100 MHz. Considering the vibration amplitude of the SAW is approximately proportional to the electrode number of the IDT, in order to increase the SAW energy, the electrode number should be large enough, such as more than 10 pairs. Meanwhile, to make the SAW field more homogeneous, the aperture of the IDTs should also be large, such as more than 20 wavelengths, thus the sizes of the IDT and the stator will be much larger. Therefore, to miniaturize the SAW motors, the frequency of the SAW should be increased to decrease the

size of the IDTs. However, the vibration amplitude should also be decreased because the SAW amplitude is approximately inversely proportional to the frequency of the IDTs. As the motors are fabricated to operate at very high frequencies, the vibration amplitudes of the SAWs are very small, so it is required that the surface of the stators should be very smooth, i.e., with very fine roughness (Takasaki et al., 1998; Cheng et al., 2002).
On the other hand, the Lamb wave is another kind of wave modes used in SAW motors, which is excited in thin piezoelectric plates (films) as shown in Fig.2(c) and is suitable for manufacturing micro-motors (micro-actuators) used in micro-electro-mechanical systems.

(b) Sliders

Generally, the sliders in SAW linear motors could be thin plates or small balls fabricated by various materials, such as silicon wafers or aluminum sheets, steel balls and/or ruby balls, etc. In order to control the contact pressure and contact area between the sliders and stators, spherical-shaped sliders may be preferably adopted. To increase the friction-driving force, it is better to manufacture the contact area of the slider with a multi-sphere shape, such as an array of small bumps at the contact surface of a silicon wafer slider, as shown in Fig. 3(c), especially for the motors operating in higher frequencies (Takasaki et al., 1998; 2000).

3.3 Characteristic and performance of SAW linear motors

The moving velocity and the output force of SAW linear motors driven by the frictional forces are dependent upon the driving voltage of the IDTs and the contact pressure between the stators and sliders. To get suitable velocity and output force of the motors, the contact pressure must be controlled by applying preload, such as applying leaf springs or magnets. For example, for a SAW motor with the frequency about 10 MHz, a Si wafer with projection array shown in Fig.3(c) was used as a slider under a leaf spring preload of about 30 N, the transient responses of the slider motion under different driving voltages were measured by a laser vibrometer as shown in Fig.4(a) (Kurosawa, 2000). Sequentially, a miniaturized SAW motor with the frequency of about 50 MHz was presented, in which the Si wafer was used as a slider and a magnetic force was used to control the preload. The moving speeds of the silicon slider under different driving voltages were measured as shown in Fig.4(b) (Takasaki et al., 1998), in which the maximum output force was calculated as 0.036 N, that is 28% of the preload,. To investigate the effect of the slider material on the transient response of the motor, three kinds of materials were used as the sliders and the results were shown as Fig.4(c) (Kurosawa et al., 1994).
Up to now, the SAW motors driven with much higher frequencies have been fabricated. For example, a motor operating at about 100 MHz has been accomplished, therefore the size of the stator was greatly reduced to $3\times12.5\times0.5$ mm^3. The results showed that the motor had a high speed of 0.3 m/s and a high output force of 13 mN (Shigematsu & Kurosawa, 2006).
To increase the efficiency of SAW motors, two kinds of power circulation methods were developed (Asai et al., 1999). The first power circulation method is shown in Fig.5(a), in which two driving IDTs and two unidirectional IDTs are required. The excited traveling wave is received by one unidirectional IDT and converted into electric energy. Another unidirectional IDT excites a circulated traveling wave using the electric energy. Each unidirectional IDT is located at a suitable position, then the excited wave and circulated wave can add up with each other. The second method is shown in Fig.5(b), in which two

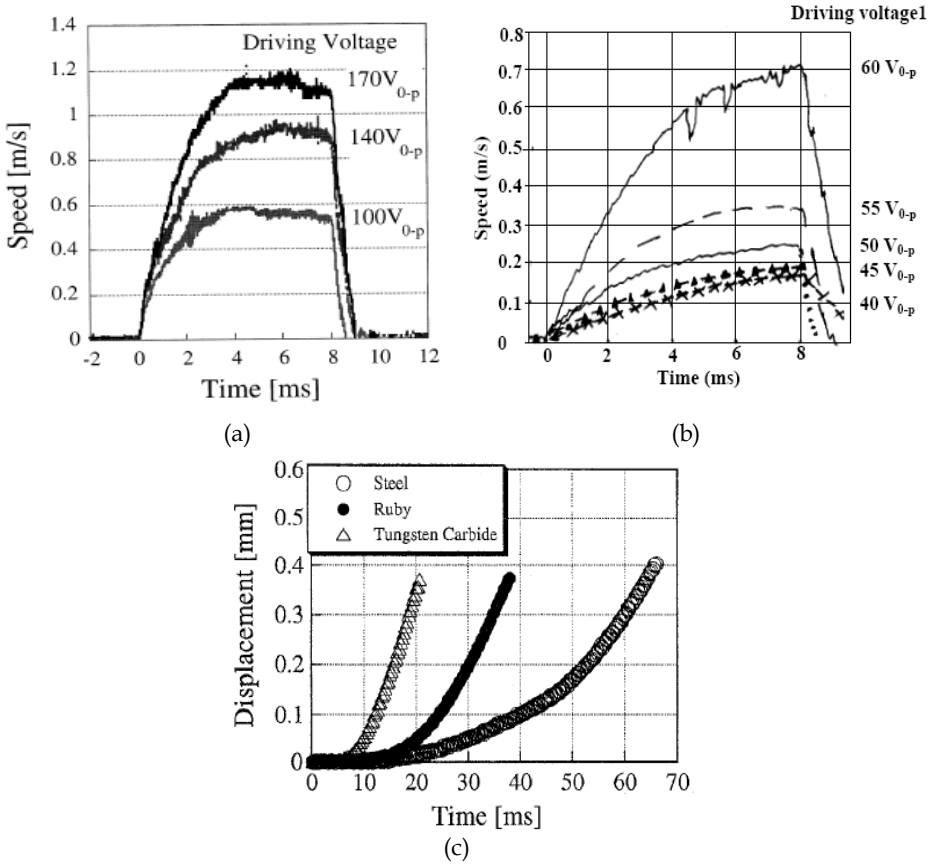

Fig. 4. Transient response of SAW motor: (a) at about 10 MHz; (b) at 50 MHz; (c) at about 10 MHz.

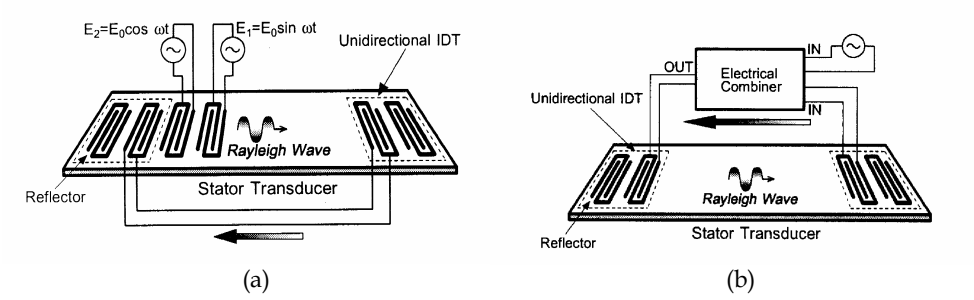

Fig. 5. Structure of stator using two power circulation methods

unidirectional IDTs and an electrical combiner are required. The output port of the combiner is connected to the exciting unidirectional IDT and the input ports are connected to the other IDT and a RF electric power source. The excited SAW is received by the other IDT and converted to electric energy, and further put into the combiner, which makes the energy to be recycled.
However, on the other hand, the abrasion is one problem that influences the lifetime of the motor driven by frictional force. To avoid the problem, segment-structured diamond-like carbon film coatings were proposed to be applied for the friction material (Fujii et al., 2007). The segment-structured film coatings could be deposited on the sliders and/or on the stators, which are available as the projections on the silicon sliders.

3.4 SAW rotary motors

On the basis of the SAW linear motors, SAW rotary motors were developed, in which two pairs of IDTs were deposited in parallel on the surface of 128^0 YX-$LiNbO_3$ substrate as the stator shown in Fig.6(a) (Zhang et al., 2000). In the stator, while IDT-1 and IDT-3 are applied a RF voltage with the central frequency of the IDTs, two SAWs with anti-parallel propagation directions are excited. As a rotor is located at the center of the stator and spans on both SAW waves, the anti-parallel propagations of both SAWs produce one pair of oppositely directed frictional forces on the rotor, which result in a torque driving the rotor to rotate in anti-clock-wise. It is easy to invert the rotation direction by using the other two IDTs (2 and 4) to excite other pair of anti-parallel SAW waves.
For the rotary motors initially built-up, the prototype using Rayleigh waves is shown in Fig.6(b), the IDTs are composed of 20 pairs interdigital electrodes with the aperture of 25 mm and the operation frequency of about 10 MHz. The rotors are circular disks, in which a series of small holes distributed axisymmetrically near the fringe, and the holes are filled with small balls as shown in Fig.6(c). The disks and balls can be made by different materials, such as plexiglass disks and steel balls, etc. The motor speeds were measured by a digital video camera and analyzed by an image processing program. As the IDTs are supplied with the driving voltage of 100 $V_{p\text{-}p}$ about 2 seconds, the angular displacement and rotation speed of the rotary motor gradually increase to about 2000 degrees (5.5 circles) and 20 rad/sec, respectively. From the transient response, the maximum torque and torque-speed relationships are estimated using the method proposed by Nakamura et al. (1991), by which it is found that the maximum output torque is 3.3 Ncm, and the steady rotation speed is 180 rpm at the driving voltage of 100 $V_{p\text{-}p}$.

4. Theoretical simulation of SAW motors

4.1 Theory and numerical simulation of linear SAW motors

The first attempt to describe the energy transfer from the acoustic wave to the slider in the linear SAW motors, perhaps, was presented by the mechanism that the slider is in alternative phase of levitation and contact with the stator, and then the slider motion is in sequential step-like behavior (Helin et al., 1998). Based on the mechanism, as the SAW motor driven by Rayleigh wave has a spherical slider, the theoretical model can be simplified as shown in Fig.7(a), in which the displacement (x_{ellip} ,y_{ellip}) of the surface particle of the stator can be expressed as (Morita et al., 1999)

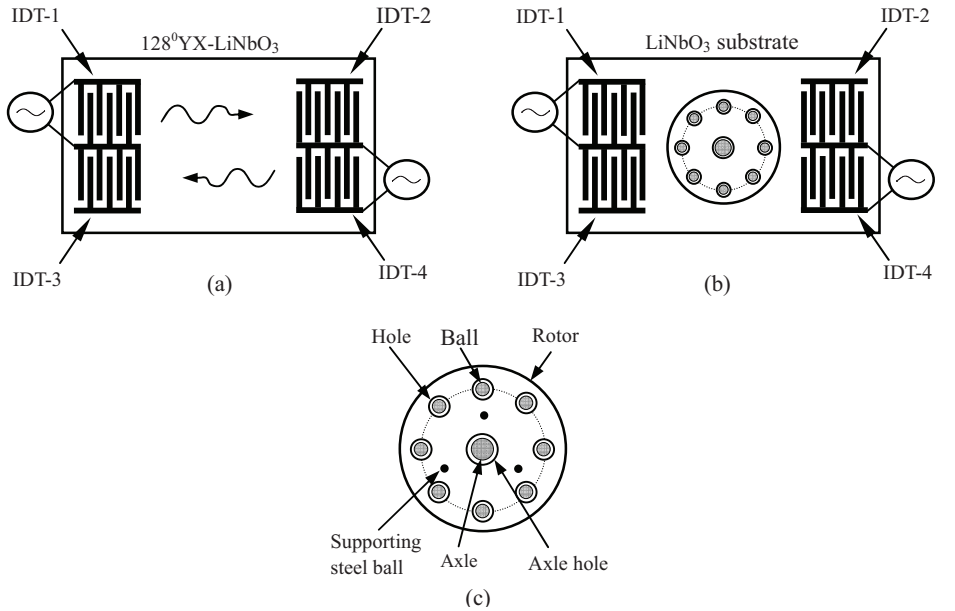

Fig. 6. Schematic diagram of the SAW rotary motor. (a) stator; (b) SAW rotary motor; (c) rotor

$$\begin{cases} x_{\text{ellip}} = A\alpha\cos(\omega t + kx_{\text{slider}}), \\ y_{\text{ellip}} = A\sin(\omega t + kx_{\text{slider}}), \end{cases} \tag{1}$$

where A is the amplitude, ω is the angular frequency, k is the wave number, α is the ratio of the tangential amplitude to the normal amplitude of the vibration, and x_{slider} and y_{slider} are the coordinate positions of the slider. During the operation, the slider experiences two situations: one is in levitation and the other is in contact with the stator as shown in Fig.7(b) and (c) respectively.

If $y_{ellip} < y_{slider}$, the slider is in levitation as shown in Fig.7(b), then the motion equations are

$$\begin{cases} Md^2 y_{\text{slider}} / dt^2 = -P - Mg, \\ Md^2 x_{\text{slider}} / dt^2 = 0, \end{cases} \tag{2}$$

where P is the preload to the slider, M is the mass of the slider, and g is the gravity.

If $y_{ellip} > y_{slider}$, the slider is in contact with the stator as shown in Fig.7(c), so it obtains a frictional force in the tangential direction. The motion equations are written as

$$\begin{cases} Md^2 y_{\text{slider}} / dt^2 = N - P - Mg, \\ Md^2 x_{\text{slider}} / dt^2 = Fv_{\text{slider}} / \left|v_{\text{slider}}\right| = \pm\mu N v_{\text{slider}} / \left|v_{\text{slider}}\right|, \end{cases} \tag{3}$$

where N is the normal supporting force in the normal direction, μ is the frictional coefficient and v_{slider} is the speed of the slider. The contact force is calculated using the Herzian contact theorem as follows (Timoshenko et al., 1970)

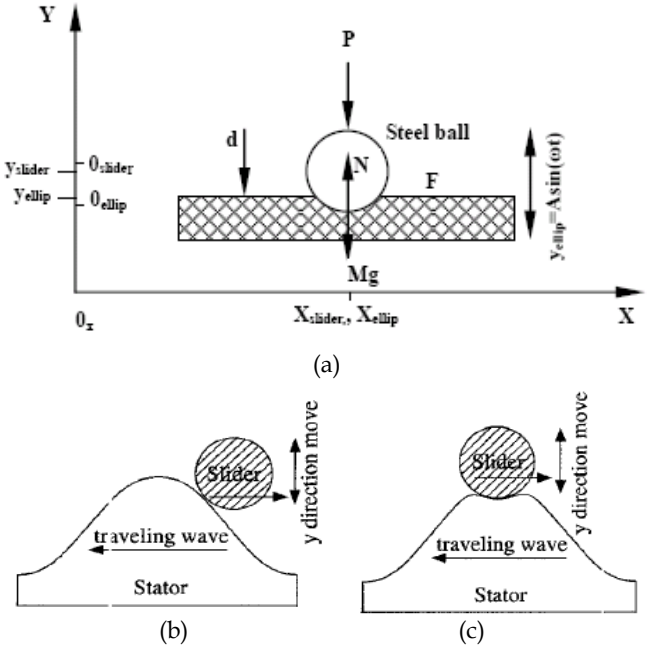

Fig. 7. Theoretical model of SAW linear motor: (a) position of slider; (b) levitation; (c) contact

$$N = \frac{4ER^{\frac{1}{2}}d^{\frac{1}{2}}}{3}, \qquad E = \left(\frac{1-\sigma_1^2}{E_1} + \frac{1-\sigma_2^2}{E_2} \right)^{-1}, \tag{4}$$

where R is the radius of the rotor, E_i and σ_i (i =1,2 represent the slider and the stator, respectively) are the Young's module and Poisson's ratio, respectively.
To calculate the displacement and speed of the slider, the Euler method is used as

$$\begin{cases} x_{slider}(t_n) = x_{slider}(t_{n-1}) + \dfrac{dx_{slider}}{dt}(t_{n-1})\Delta t, \\ v_{slider}(t_n) = v_{slider}(t_{n-1}) + \dfrac{dv_{slider}}{dt}(t_{n-1})\Delta t. \end{cases} \tag{5}$$

The simulation results for the motor driven by a pulse-modulated force with the frequency of 9.6 MHz are shown in Fig.8, where the left (Fig.8(a)) depicts the driving force, while the middle and right show the moving speed and the displacement respectively (Morita et al., 1999). The results are in agreement with those of the experiments.
Recently, further studies on the friction-driven SAW motors have been reported in details including the measurements, analyses, modeling, physics of contact, and design criteria, which were published in five papers separately (Shigematsu & Kurosawa, 2008a; 2008b; 2008c; 2008d; 2008e). It is clearly that these papers provide a systematical information, experiments and theories for optimizing the designs, manufactures and applications of the friction-driven SAW motors.

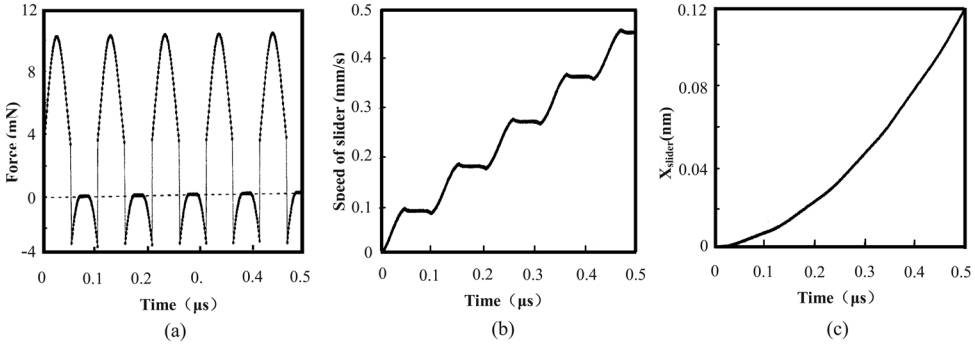

(a) (b) (c)

Fig. 8. Numerical simulations of transient response for linear motor: (a) driving force; (b) moving speed; (c) displacement

4.2 Rotary motor

On the basis of the theoretical model of the linear motors, the similar theoretical model of the rotary motors has been constructed (Cheng et al., 2002; 2003a; 2003b). Owing to the axisymmetry, only two balls at the fringe of the rotor are considered for simplicity as shown in Fig.9(a).

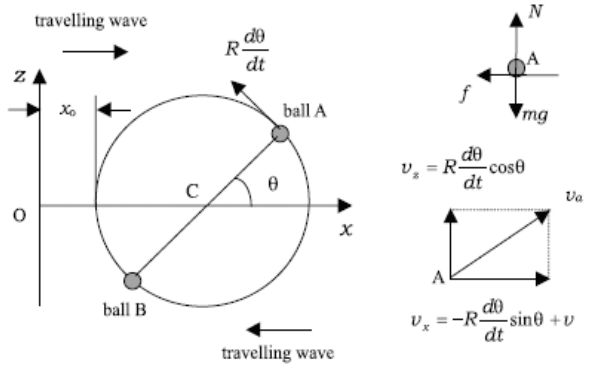

(a)

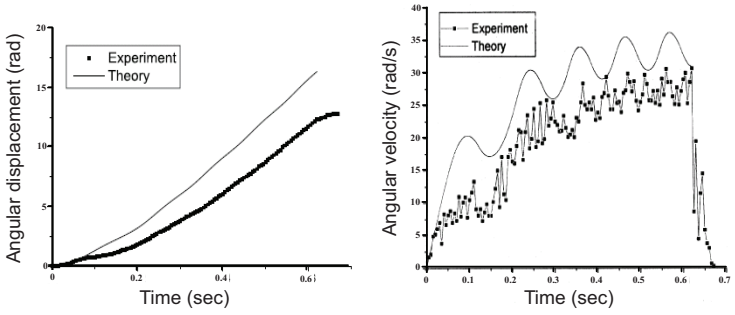

(b) (c)

Fig. 9. Numerical simulations of rotary motors: (a) theoretical model; (b) angular displacement versus time; (c) anglular velocity versus time.

When the ball is levitating, the motion equations are as

$$\begin{cases} md^2y_{ball} / dt^2 = -mg, \\ Id^2\theta / dt^2 = -M, \end{cases} \tag{6}$$

where m is the mass of the ball, I is the moment of inertia of the rotor with respect to the axis. When the ball is contacting the stator, the motion equations are

$$\begin{cases} m\dfrac{d^2y_{ball}}{dt^2} = N - mg, \\ I\dfrac{d^2\theta}{dt^2} = 2\mu N \dfrac{(v - R\dfrac{d\theta}{dt}\sin\theta)R\sin\theta - R\dfrac{d\theta}{dt}\cos\theta \cdot R\cos\theta}{\sqrt{(R\dfrac{d\theta}{dt}\cos\theta)^2 + (v - R\dfrac{d\theta}{dt}\sin\theta)^2}} - M, \end{cases} \tag{7}$$

where R is the radius of the rotor. The supporting force on the ball is calculated as

$$N = \frac{4Er^{\frac{1}{2}}d^{\frac{1}{2}}}{3}, \qquad E = \left(\frac{1-\sigma_1^2}{E_1} + \frac{1-\sigma_2^2}{E_2}\right)^{-1}, \tag{8}$$

where r is the radius of the small ball.

For the rotary motor with the SAW frequency of 30 MHz, the experimental and theoretical results of the angular displacement and speed are shown in Fig.9(b) and (c) (Cheng et al., 2002). From the figure, it can be seen that the simulation results are roughly consistent with the experimental results with slight deviations, which might be induced by the following reasons: the friction between the axis and the rotor is neglected and, especially, only two balls' motions are considered in the theoretical calculations for simplicity. Further calculations showed that as the number of the balls increases, the rotary motion is more stable and closer to that of the experiments (Cheng et al., 2003b).

5. Non-contact SAW motors and actuators

The SAW motors described above are driven by the frictional forces generated by direct contact between the sliders (or rotors) and the stators, which restrict the motion velocity and working lifetime of the motors. On the other hand, as the amplitude of the SAW decreases to less than the surface roughness of the stators, it is not possible to drive the motors by the frictional force. In order to overcome the deficit of the friction-driven motors and expand the application fields of the motors, non-contact SAW motors were proposed, in which a fluid layer is introduced in the interface between the stator and slider (rotor). As a high frequency voltage is supplied to the IDT which is deposited on the stator, the SAW (Rayleigh wave) will be excited by the IDT, which further radiate longitudinal waves in the fluid media between the slider (rotor) and stator. As the second-order effect of the wave propagation, the acoustic streaming is induced, whose viscous force drives the slider (rotor) to move.

5.1 SAW streaming

When acoustic waves travel through a medium, if the acoustic intensity is not high, the acoustic wave propagation is a linear phenomenon, i.e., only the acoustic energies propagate, the medium does not move globally. However, as the wave amplitude increases, the nonlinear effect appears, and an interesting feature of the sound field, i.e., the medium presents steady motions, becomes evident. Such a nonlinear phenomenon is called "acoustic streaming" (Nyborg, 1958; 1965). These flows can be generated around the surfaces of obstacles immersed in intensive acoustic fields and/or vibrating elements and near bounding walls. Similarly, when SAWs (Rayleigh waves) with high intensity reach the boundary between fluids and solids, the transmission mode is changed from the Rayleigh mode to the leaky Rayleigh mode. Meanwhile, the leaky Rayleigh waves radiate the acoustic energy in the fluid, and then the fluid is driven to move, which is called "SAW streaming" because the phenomenon involves essentially the same physics as the "acoustic streaming" (Shiokawa et al., 1990).

(a) Experiment of SAW streaming

The Rayleigh wave can readily radiate a longitudinal wave into a fluid when the surface with the Rayleigh wave propagation is in contact with a fluid layer. When the fluid volume is small and the acoustic power increases above a certain threshold, the fluid begins to move in the direction of the SAW propagation, which provides an observable pattern of the SAW energy flow. Moreover, if the substrate surface is hydrophobic, a lot of droplets are expelled from the liquid surface as shown in Fig.10 (Shiokawa et al., 1989; 1995; Uchida et al., 1995).

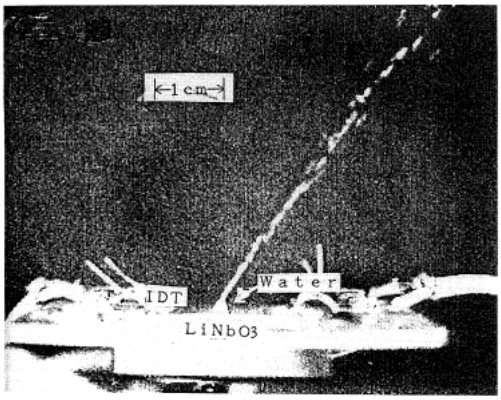

Fig. 10. Water jet streaming excited by SAW.

(b) Theory of SAW streaming

The general equation of hydrodynamics of viscous fluids is as follows (Shiokawa, et al., 1990):

$$F = -\nabla P + \eta \nabla^2 v + \frac{1}{3}\eta \nabla(\nabla \cdot v), \tag{9}$$

where F is the net force per unit volume due to stress, ρ is the density, η is the shear viscosity coefficient and v is the particle velocity.

Based on the continuity equation, one can obtain:

$$\frac{\partial(\rho v)}{\partial t} + \rho(v \cdot \nabla)v + v\nabla \cdot \rho v = F_0 - F_1, \tag{10}$$

where

$$F_0 = \frac{\partial(\rho v)}{\partial t}, \quad -F_1 = \rho(v \cdot \nabla)v + v\nabla \cdot \rho v. \tag{11}$$

For acoustic waves vary sinusoidally with time at the frequency ω, in order to obtain a streaming equation from Eqs. (10) and (11), it is need to retain the terms up to the second order and take the time average over a suitable number of cycles. Noting that the time average of F_0 should be zero in the steady state, then

$$-F_1 = \left\langle \rho_0(v \cdot \nabla)v + v\nabla \cdot \rho_0 v \right\rangle, \tag{12}$$

in which $\langle\ \rangle$ means "time average", and F_1 is the exact force of the acoustic streaming.

5.2 Non-contact SAW linear motors and actuators

(a) Initial non-contact SAW linear motors

The first non-contact linear SAW motor (manipulator) using Rayleigh wave was proposed as shown in Fig.11(a), in which a liquid droplet is put on the surface of the stator and a small slider is placed on the liquid droplet (Sano et al., 1997). The propagating SAW drives the liquid droplet to move in the SAW propagation direction by SAW streaming, and the slider moves with the droplet together. For the motors with different frequencies, the amplitude of the Rayleigh waves measured by a laser probe and normalized by the wavelength versus the driving voltage is shown in Fig. 11(b), and the dependence of moved distance of the slider on the voltage is shown in Fig. 11(c), which shows that the motors are suitable to be used as non-contact actuators, such as micromanipulators.

(b) New type of non-contact SAW linear motors

Recently, a new type of non-contact SAW motors was proposed, in which a thin liquid layer surrounded by a thin glass wall was put on the surface of the stator as shown in Fig.12(a). In the experiments, two kinds of IDTs with different frequencies and sizes were deposited, and the effects of the SAWs with different frequencies on the performances of the non-contact motors were studied (Gu et al., 2009).

5.3 Theoretical model of non-contact SAW linear motors

If the SAW propagation surface is in contact with liquid, based on the ultrasonic wave radiation mechanism, an approximate theoretical model is developed as shown in Fig.12(b). In the liquids (z > 0), the particle displacement (u_x, u_z) can be written as (Shiokawa et al., 1989)

$$\begin{aligned} u_x &= A \exp j\omega t \cdot \exp(-jk_L x) \cdot \exp(-\alpha k_L z) \\ u_z &= -j\alpha A \exp j\omega t \cdot \exp(-jk_L x) \cdot \exp(-\alpha k_L z), \\ k_L &= \omega / V_L, \alpha^2 = 1 - (V_L / V_W)^2. \end{aligned} \tag{13}$$

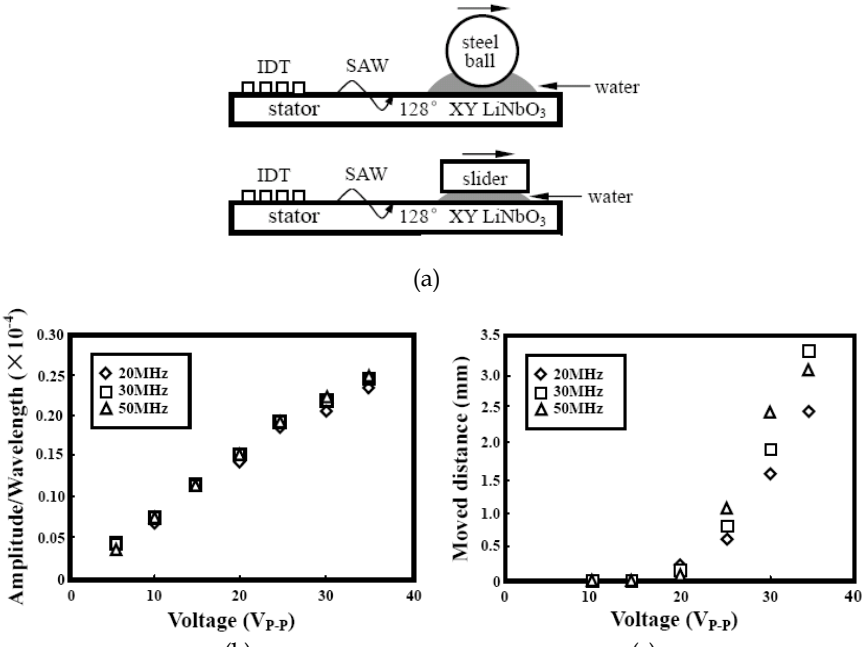

Fig. 11. SAW manipulator: (a) schematic diagram; (b) amplitude/wavelength VS voltage; (c) distance VS voltage.

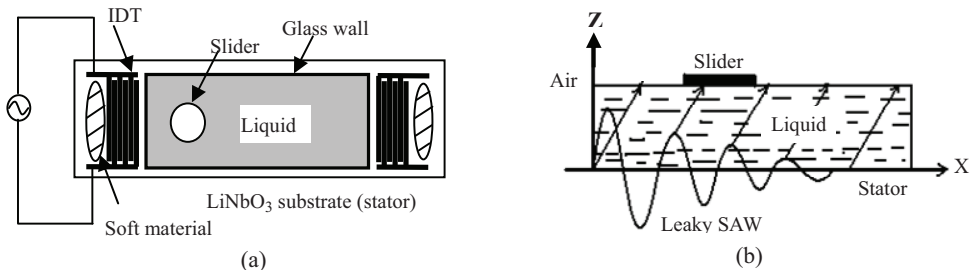

Fig. 12. Non-contact SAW linear motors: (a) schematic diagram of structure; (b) theoretical model

where A is the horizontal vibration amplitude of the particle, ω is the angular frequency (for simplicity, the SAW harmonics are neglected), K_L is the wave number, and a is a complex propagation constant of the leaky SAW, V_L and V_W are the velocities of the leaky SAW and longitudinal wave of the liquid, respectively. V_L can be calculated by applying a perturbation method, which treats the leaky wave as a first-order perturbation on the non-leaky wave propagation, and assuming the boundary conditions satisfy that both the displacement and the stress are continuous at the interface between the liquid and solid substrate (z = 0) (Campbell & Jones, 1970).

According to the theory of near-boundary acoustic streaming, the basic equations used for the streaming are (Nyborg, 1958; Shiokawa et al., 1990)

$$\vec{F} = -\rho_0 \langle \vec{U}_1 \cdot \nabla \vec{U}_1 + \vec{U}_1 \nabla \cdot \vec{U}_1 \rangle , \tag{14}$$

$$\mu \nabla^2 \vec{U}_2 - \nabla \vec{P}_2 + \vec{F} = 0 , \tag{15}$$

where ρ_0 and μ are the density and viscosity of the fluid respectively, the bracket indicates a time average over a large number of cycles, $\vec{U}_1$ is the particle velocity of the stator surface, $\vec{U}_2$ is the streaming velocity, and $\vec{P}_2$ is the acoustic pressure of the liquid at the interface between the liquid and stator. Both $\vec{U}_2$ and $\vec{P}_2$ are time-independent second-order perturbation quantities as the effect of the viscosity of the liquid (such as water) is ignored, $\vec{F}$ is the acoustic streaming force, which is a nonlinear quantity.

Substituting the x and z components of $\vec{U}_1$, i.e., u_x and u_z of Eq. (13), into Eqs. (14), the x and z components of $\vec{F}$, i.e., F_x and F_z, are given by

$$\begin{aligned} F_x &= -\rho_0 (1+\alpha_1^2) A^2 \omega^2 k_i \exp 2(k_i x + \alpha_1 k_i z) \\ F_z &= -\rho_0 (1+\alpha_1^2) A^2 \omega^2 \alpha_1 k_i \exp 2(k_i x + \alpha_1 k_i z) \end{aligned}, \tag{16}$$

where α_1 and k_i are the imaginary parts of α and k_L, respectively. F_z does not contribute to the motion of the slider, so the F_x is just considered as the force acting on the levitated slider. Since k_i is always a minus value, F_x is attenuated with the distance x.

The following analyses are conducted with the model shown in Fig.12(b), in which the thickness of the liquid is z_0 and the acoustic streaming force acted on the slider in x direction is $F_x(z_0)$. As the slider is with the area L^2 and thickness h, considering the thickness of the slider is generally very small compared with the acoustic wavelength, the acoustic streaming force is constant in the thickness range of the slider. Thus the acoustic streaming force acted on the slider at x position, $F_{sum}(x)$, is given by:

$$F_{sum}(x) = Lh \int_x^{x+L} F_x(z_0) dx. \tag{17}$$

Therefore, the acceleration of the slider at x position is given by:

$$a = \frac{F_{sum}(x)}{\rho_s h L^2} , \tag{18}$$

where ρ_s is the density of the slider.

Considering the resistant force of the liquid, there is a threshold force $F_t(x)$ for the slider starts to move, i.e., only as the horizontal vibration amplitude $A > A_r$, the streaming force can drive the slider to move, then the acceleration can be rewritten as

$$a = \frac{F_{sum}(x) - F_t(x)}{\rho_s h L^2}. \tag{19}$$

According the acceleration, the transient velocity of the slider can be obtained, so as the displacement.

5.4 Experimental and theoretical results

In the experiments, the substrates of the SAW delay lines (stators) are 128^0 YX-$LiNbO_3$ piezoelectric crystals with the size of about 75 ×18 ×1 mm^3. On the substrates, two kinds of IDT pairs with different frequencies and sizes are fabricated for studying the effects of the operation frequency on the performance of the non-contact motors (Gu et al., 2009). In the first type of the motors, the IDT has 20 pairs of electrodes with the aperture of 12 mm and the central frequency of about 10 MHz, where a rectangular cell (31.3 ×12.8 ×12 mm^3) surrounded by thin glass walls with the thickness of 0.8 mm is put on the surface of the stator to contain the liquid (water) layer. The other type has 45 pairs of electrodes with the aperture of also 12 mm and the central frequency of about 24 MHz, and a rectangular cell with the size of 31.2 ×12 ×12 mm^3 is used. The exciting voltage $V_{p\text{-}p}$ of the IDT can be adjusted in the range of 0-140 V. The slider is a circular aluminum slice with the diameter of 6 mm, the thickness of 0.24 mm, and the density of 2.7 g/cm^3. The thickness of the liquid layer between the stator and slider can be adjusted in the range of 1-8 mm.

The motion (displacement) of the slider is recorded by a high-speed digital video camera, and then the data of the motion are extracted and processed by a computer. Thus the transient velocity of the sliders can be measured and calculated. Since the transient velocity in fluctuating, the average of the transient velocities is taken as the moving velocity of the slider. According to the results, the first motor with the frequency about 10 MHz has faster transient velocity than the second one (about 24 MHz).

(a) Transient velocity versus time

For the first motor, the transient velocity of the slider is obtained as shown in Fig. 13(a), in which the thickness of the liquid (water) layer is about 3.2 mm and the driving voltage $V_{p\text{-}p}$ is 21.2 V. From Fig.13(a) it can be seen that the transient velocity increases very fast at first (about 0.1 second), and then approaches to saturation with slight oscillations. The oscillation may be induced by the vortical flows and the measurement errors. For the second motor, similar results can also be obtained, however, in order to obtain the same transient velocity at the same thickness of the water layer, the exciting voltage $V_{p\text{-}p}$ should be about 79.2 V.

(b) Velocity of slider versus exciting voltage

The velocity variations of the slider with the exciting voltages of the motors are investigated. For the first motor, as the thickness of the liquid (water) layer is about 4.0 mm, the result is shown in Fig.13(b), in which the threshold voltage V_t is about 12 V. When the exciting voltage $V_{p\text{-}p}$ increases from 12 V to 60 V, the velocity increases linearly essentially, but the velocity increases with a little slower in the lower voltage range (less than 30 V). Similarly, for the second motor, the threshold voltage V_t is about 20 V, and the velocity of the slider increases approximately linearly with the voltage in the range of 80 – 120 V, although in the lower voltage range (20 – 80 V), the increasing tendency of the velocity is slower. Since the experimental conditions are very complicated, such as the reflections of waves by the glass walls of the cell and so on, the experimental errors are always in the range about 10%.

Generally speaking, the velocity varying behavior against the exciting voltage of the SAWs is similar for both motors with different frequencies. There exists a limited threshold voltage, below which the sliders cannot move. As the voltages are larger than the threshold, the velocity of the sliders increases with the exciting voltage approximately in linear way, although the increase is more like exponential in the lower voltage range.

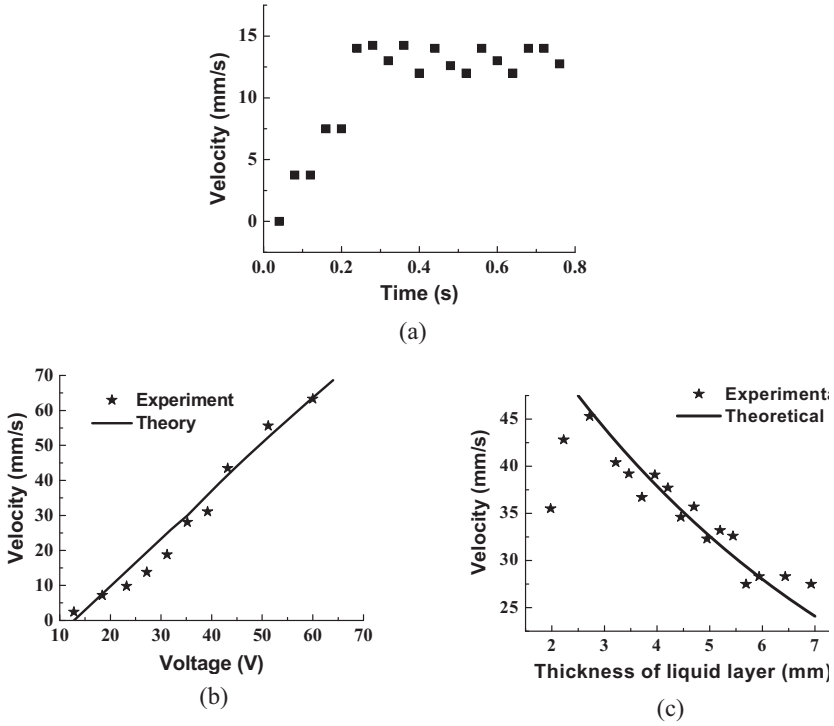

Fig. 13. Velocity of non-contact SAW linear motor: (a) transient velocity; (b) average velocity VS voltage; (c) average velocity VS thickness of liquid layer (f=9.959 MHz)

In the theoretical simulations, taking V_L = (3931 + j67.7) m/s and V_W = 1500 m/s (Campbell & Jones, 1970; Shiokawa et al., 1989), the relation between the slider velocity and the amplitude of the SAW for the motor can be obtained by Eqs.(16) - (19). Considering the amplitude of the SAW is proportional to the exciting voltage (Sano et al., 1997), the relation between the slider velocity and the exciting voltage for both motors can be obtained, one of which is shown in Fig.13(b), which shows that the slider velocity increases linearly with the exciting voltage as the voltage is beyond the threshold. It demonstrates that the theoretical result is essentially in agreement with that of the experiments.

Compared with the performance of the contact SAW motors, it can be found that the driving voltage for the non-contact motors is reduced distinctly. Therefore, the moving velocity and lifetime can be increased greatly.

(c) Slider velocity versus thickness of liquid layer

The relation between the slider velocity and the thickness of the liquid (water) layer for both motors is also studied experimentally and theoretically. In the experiments, it is found that the varying tendency of the slider velocity versus the thickness of the liquid layer for both motors is very similar. The result of the first motor is shown in Fig.13(c), which shows that, when the thickness of liquid (water) layer is larger than 3 mm, the velocity of the slider decreases exponentially with the increasing thickness of the water layer. However, as the thickness of the water layer is less than 3 mm, the slider velocity reduces with the

decreasing thickness of the water layer, which might be attributed to that the viscous drag effect increases when the thickness of the water layer gradually becomes small (Betchov & Criminale, 1967). As a result, while the thickness of the water layer increases gradually in the range of 0 – 3 mm until the liquid flow becomes stability, the velocity of the slider becomes faster. Besides, as the liquid layer thickness is less than 1 mm, the slider cannot be driven to move by the exciting voltage (V_{p-p}) of 50 V. In this case, the slider may be sometimes in contact with the stator since the liquid layer is too thin. It is also implied that the slider motion of the non-contact SAW motors is driven much easier than that of the contact SAW motors with the same SAW devices (stators).
Meanwhile, the theoretical simulations are also accomplished by suitably selecting the relevant parameters. The simulated result for the first motor is also plotted in Fig.13(c). It can be seen that the theoretical result is in good agreement with that of the experiment.

5.5 Non-contact SAW rotary motor

On the basis of the friction-driven rotary motors, non-contact rotary motors were developed, in which the same rotors and substrates are used as in contact motors. Similarly, the rotor is suspended in a thin liquid layer filled in a liquid cell located on the stator, and the angular displacement and angular speed are measured in different driving voltages as shown in Figs.14(a) and (b). In addition, to study the influence of the viscosity of the liquid layer, the mixed liquids composed of water and glycerine with different ratios are used, and the dynamic viscosity is measured by a viscometer. As the operating frequency is 9.845 MHz, the dynamic response is obtained at different times as shown in Fig. 14 (a), the angular speed changing with the driving voltage and the dynamic viscosity of the liquid are also obtained as shown in Figs.14(b) and (c), respectively. The related theoretical study is in progress.

6. Microactuator driven by different SAW modes

6.1 Microactuators driven by Lamb waves

An initial micromotor using a Lamb wave (flexural plate wave) has been presented, in which the stator is a ZnO film (1μm) deposited on Si_3O_4 film (2 μm) and both films are deposited on a Si wafer, and then the related area of Si wafer is etched as shown in Fig.15 (Moroney et al., 1989). A small polysilicon slice put on the Si_3O_4 film is driven by the Lamb wave excited by IDT fabricated on the ZnO film, the polysilicon slice can move linearly or rotationally as the Lamb waves are excited or reflected in different directions. This kind of motors can be used in MEMS technology.
Furthermore, since Lamb wave devices are able to operate in fluids (water), a fluid motion (SAW streaming) produced by Lamb waves excited by IDT at the composite of Si_3O_4 and ZnO membrane with the thickness of 4 μm was also observed (Moroney et al., 1991). The velocity of the flexural plate wave is much lower than the sound velocity in fluids (water), thus the structure acts as nearly lossless acoustic waveguides. Then the fluorescent polystyrene spheres with the diameter about 2.5 μm are put in the fluid to make the motion visible. The observed pumping speed is proportional to the square of the wave amplitude, the speed was 100 μm/s for a RF driving voltage of 8V and a wave amplitude of 6.5 nm. A nonlinear model based on acoustic streaming theory was presented to predict the velocities, which was in good agreement with the experiments.

In addition, some other micromachined actuators have also been presented by several groups, where ultrasonic flexural plate waves traveling along thin piezoelectric membranes were used to excite acoustic fields in the fluids contacted with the membranes (Luginbuhl et al., 1998; Meng et al., 2004). These kinds of microactuators have been used for transportation of particles and/or droplets in micro-biological research fields.

6.2 Micromanipulators driven by leaky waves

Practically, micromanipulators using leaky waves in thin liquid layers produced by SAW devices with very high frequency about 100 MHz were fabricated by several groups. One of them is shown in Fig. 16 (Takeuchi et al., 1994), where the tip of the substrate of the Rayleigh wave device was immersed with a Rayleigh angle in a liquid layer (or drop). At the interface of the substrate and liquid, the SAW is converted to leaky waves, which then become longitudinal waves in the liquid. As the wave intensity is high, the acoustic streaming (or radiated force) drives small glass particles to move in 1- or 2-dimensional way in the liquid if there are two pairs of SAW devices located perpendicular to each other. It can be used in bioengineering and micromachining (Renaudin et al., 2006).

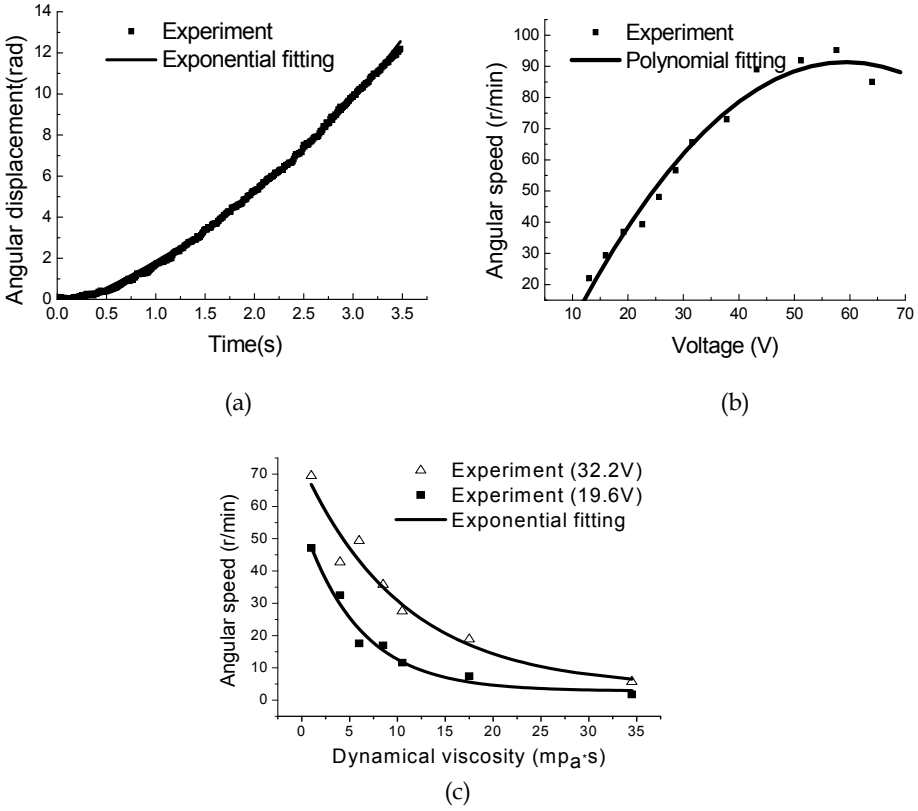

Fig. 14. Response of non-contact rotary motor: (a) angular displacement VS time; (b) angular speed VS voltage; (c) angular speed versus the dynamical viscosity of liquid layer

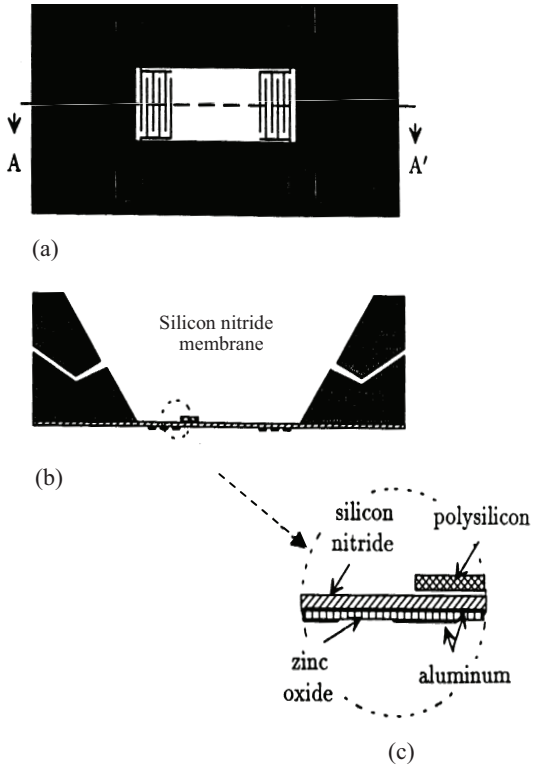

Fig. 15. Micromotor driven by Lamb wave: (a) back side; (b) cross section; (c) enlarged pattern of circle in (b)

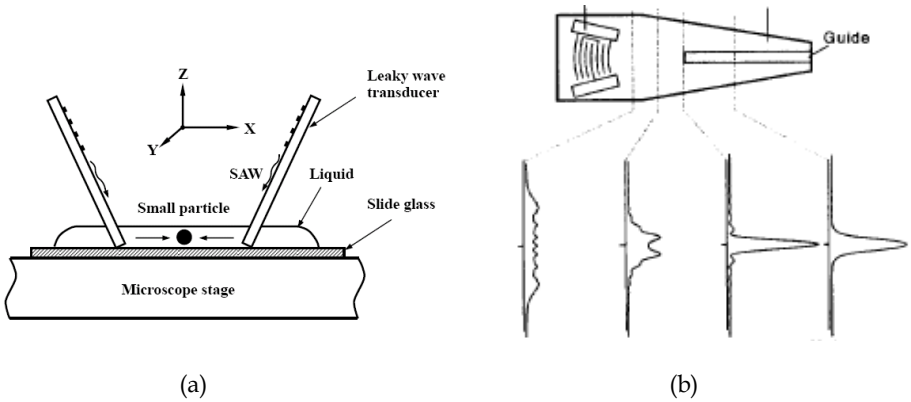

Fig. 16. Manipulator driven by leaky wave: (a) sketch of set up; (b) SAW device and corresponding acoustic field

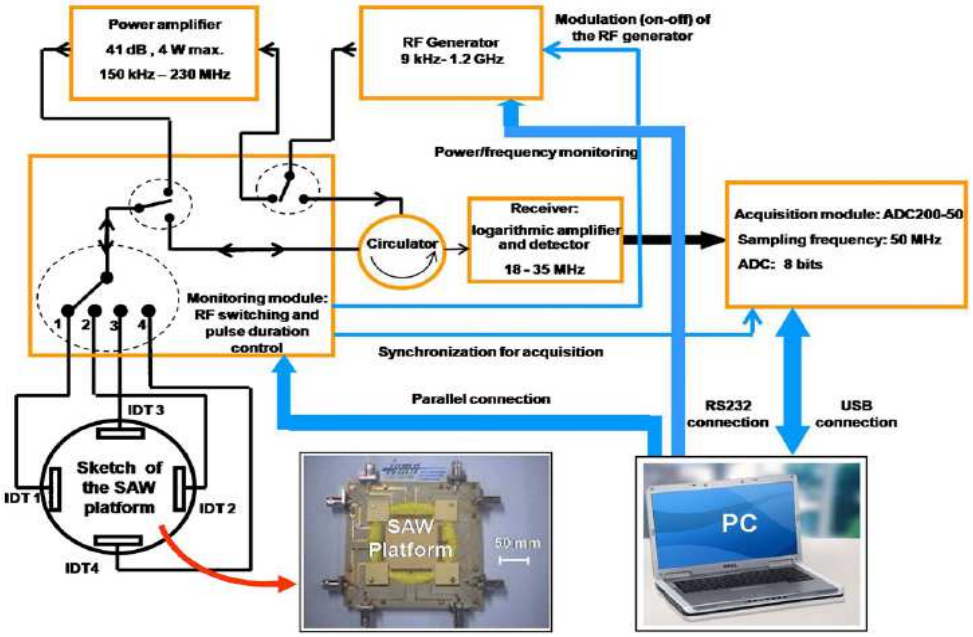

Fig. 17. Schematic diagram of SAW actuator system used for tracking microdroplet.

7. Potential applications

Apparently, the SAW motors and actuators have wide applications in micro-electro-mechanical systems and biological sciences and technologies. As examples, the motors would be capable of operating in multiple degrees of freedom, such as two dimensional translation stages and self-actuated spherical joints to be rotated about two orthogonal axes, which are amenable to integrate into diverse structures and machines, such as robots (NASA Tech Briefs, 2003). Practically, SAW-actuated devices have also been used for drop translation, microchannel pumping, drop manipulation, micromixing, microparticle collection and concentration, forming specific examples of the potential of technology, as lab-on-a-chip devices for microarray technology and rapid bioscaffold cell seeding, etc. (Qi et al., 2008). Meanwhile, the acoustic streaming has also been used in atomization systems.
As an example, a set up of SAW actuator used for tracking droplets is shown in Fig. 17 (Renaudin et al., 2009).

8. Conclusion

The conventional linear and rotary motors driven by IDT-excited SAWs in the frequency range of 1–100 MHz have been introduced briefly. For the conventional SAW motors, the sliders (or rotors) and the stators are in direct contact, and the driving mechanism is the frictional force between the sliders (rotors) and the stators. On the other hand, a new type of noncontact motors has been developed. Instead of the frictional forces, the acoustic streaming, which is excited by SAWs propagating in the fluids covered on the surfaces of the stators, is used to drive the sliders.

The SAW motors as micro-actuators will be very useful in advanced industrial technologies and/or biotechnical engineering due to their various advantages, such as very short response time, low driving voltage, large output force or torque, miniaturized size, easy control and batch production, etc.

On the other hand, several theoretical models have been presented and the numerical simulations for the motors and actuators in contact and noncontact types have also been performed. The theoretical results are in good agreement with those of the experiments, which demonstrate that the theoretical models can well be used to explain the working mechanism of the motors (actuators). Therefore, by combining the theoretical models and experimental results, the constructions and the performances of various SAW motors (actuators) can be optimized.

9. Acknowledgements

This work is supported by national natural science foundation of china (grant no. 10774074 and no. 10874083).

10. References

Asai, K.; Kurosawa, M. K. & Higuchi, T. (1999) Novel power circulation methods for a surface acoustic wave motor, *IEEE Ultrasonic Symposium Proceedings*, 667-670.

Auld, B. A. (1973) *Acoustic Fields and Waves in Solids*, A Wiley-Interscience Publication, John Wiley & Sons, New York, USA.

Betchov, R.& Criminale, W. O. J. (1967) *Stability of parallel flows*, Academic Press, New York, USA

Campbell, J. J. & Jones, W. R. (1070) Propagation of surface waves at the boundary between a piezoelectric crystal and a fluid medium, *IEEE Transaction on Sonics and Ultrasonics*, Vol. SU-17, 71-76.

Cheng L. P.; Zhang G. M.; Zhang S. Y.; Yu J. & Shui X. J. (2002), Miniaturization of surface acoustic waves rotary motor, *Ultrasonics*, Vol. 39, 591-594.

Cheng, L. P.; Zhang, G. M.; Zhang S. Y.; Zhang Z. N. & Shui X. J. (2003a) Theoretical simulation of a rotary motor driven by surface acoustic waves, *Acoustical Physics*, Vol. 49, 194-198.

Cheng, L. P.; Zhang, G. M.; Zhang S. Y.; Yu J. & Shui X. J. (2003b) Study of surface acoustic wave rotary motors, *Chinese Journal of Acoustics*, Vol.20, 323-328.

Cheng, L. P. & Zhang, S.,Y. (2007) Simulation of the flow induced by acoustic streaming in noncontact ultrasonic motors, *Applied Physics Letters*, Vol. 90, 244106.

Dong, S.; Wang, S.; Shen, W. & Li, L. (2000) A miniature piezoelectric ultrasonic motor based on circular bending vibration mode, *ASME Transactions on Mechanics*, Vol. 5, 325-330.

Fujii, Y.; Kotani, H.; Masaya, T.; Mizuno, T.; Aoki, Y.; Adachi, Y. & Ohtake, N. (2007) Surface acoustic wave linear motor using segment-structured diamond-like carbon films on contact surface, *IEEE Ultrasonic Symposium Proceedings*, 2543-2546.

Gu, H.H.; Cheng, L.P.; Zhang, S.Y.; Zhou, F. M. & Shui, X. J. (2008) Experimental Study on non-contact linear motors driven by surface acoustic waves, *IEEE Ultrasonic Symposium Proceedings*, 1835-1837.

Gu, H.H.; Zhang, S.Y.; Cheng, L.P.; Ma, D.; Zhou, F. M.; Chen, Z. J. & Shui, X. J. (2009) Study on non-contact linear motors driven by surface acoustic waves, *Sensors and Actuators*, A155, 163-167.

Helin, P.; Sadaune, V. & Dron, C. (1998) Theoretical and experimental study of linear motors using surface acoustic waves, *Sensors and Actuators* A, Vol. 70, 67-74.

Hu, J. H.; Yamazaki, T.; Nakamura & Ueha, S. (1995) An analysis of a noncontact ultrasonic motor with an ultrasonically levitated rotor, *Japanese Journal of Applied Physics*, Vol. 34, 2702-2706-

Koster, D. (2007) Numerical simulation of acoustic streaming on surface acoustic wave-driven biochips, *SLAM Journal on Scientific Computing*, Vol. 29, 2352-2380.

Kurosawa, M.; Takahashi, M. & Higuchi, T. (1994) An ultrasonic X-Y stage using 10 MHz surface acoustic wave, *IEEE Ultrasonic Symposium Proceedings*, 535-538.

Kurosawa, M., Takahashi, M. and Higuchi, T., (1996) Ultrasonic linear motor using surface acoustic waves, *IEEE Transaction on Ultrasonics, Ferroelectronics, and Frequency Control*, Vol. 43, 901-906.

Kurosawa, M. K., (2000) State-of-the-art surface acoustic wave linear motor and its future applications, *Ultrasonics*, Vol. 38, 15-19.

Luginbuhl, Ph.; Collins, S. D.; Racine, G. A.; Gretillat, M. A.; de Rooij, N. f.; Brooks, K. G. & Setter, N. (1998) Ultrasonic flexural Lamb-wave actuators based on PZT thin film, *Sensors and Actuators*, Vol. A 64, 41-49.

Meng A. H.; Nguyen N. T. & White R. M., (2004) Focused flow micropump using ultrasonic flexural plate waves, Biomedical Microdevices, Vol. 2, 169-174.

Morita, T., Kurosawa, M. K. and Higuchi, T., (1999) Simulation of surface acoustic wave motor with spherical slider, *IEEE Transactions on Ultrasonics, Ferroelectrics, and Frequency Control*, Vol. 46, 929-934.

Moroney, R. M.; White, R. M. & Howe, R. T. (1989) Ultrasonic micromotors: physics and application, *IEEE Ultrasonic Symposium Proceedings*, 745-748.

Moroney, R. M.; White, R. M. & Howe, R. T., (1991) Microtransport induced by ultrasonic Lamb waves, Applied Physics Letters, Vol. 59, 774 - 776

Nakamula, K.; Ito, T., Kurosawa, M. & Ueha, S. (1990) A trial construction of an ultrasonic motor with fluid coupling, *Japanese Journal of Applied Physics*, Vol. 29, L160-L161.

Nyborg, W. L. (1958) Acoustic streaming near a boundary, *The Journal of the Acoustical Society of America*, Vol. 30, 329-339.

Nyborg, W. L. (1965) Acoustic streaming. In: *Physical Acoustics*, Mason W. P. (Ed), Vol. 2B, 265–283, Academic Press, Englewood Cliffs, USA,.

Qi, A.; Yeo, L.Y. & Friend, J.R. (2008) Interfacial destabilization and atomization driven by surface acoustic waves, *Physics of Fluids*, Vol. 20, 074103-1-14.

Renaudin, A.; Tabourier, P.; Camart, J. C.& Druon, C. (2006) Surface acoustic wave two-dimensional transport and location of microdroplets using echo signal, *Journal of Applied Physics*, Vol. 100, 161101)

Renaudin, A.; Sozanski, J. P.; Verbeke, B.; Zhang, V.; Tabourier, P. & Bruon, C. (2009) Monitoring SAW-actuated microdroplets in view of biological applications, *Sensors and Actuators* B, Vol. 138, 374-382.

Sakano K, Kurosawa M. K., Shigematsu T., (2008) Surface acoustic wave motor with flat plane slider, *International Symposium on Micro-Nanomechatronics and Human Science*, 243-248.

Sano, A.; Matsui, Y. & Shiokawa, S. (1997) A new manipulator based on surface acoustic wave streaming, *IEEE Ultrasonic Symposium Proceedings*, 467-470.

Sashida, T. & Kenjo, T. (1993) *An introduction to ultrasonic motors*, Oxford University Press Inc., New York, USA.

Shigematsu, T. & Kurosawa, M. K. (2006) Miniaturized SAW motor with 100 MHz driving frequency, *IEE Japanese Transactions on Sensors and Micromachines*, Vol. 126, 166-167.

Shigematsu, T. & Kurosawa, M. K. (2008a) Friction drive of an SAW motor. Part I: Measurements, *IEEE Transactions on Ultrasonics, Ferroelectrics, and Frequency Control*, Vol.55, 2005-2015.

Shigematsu, T. & Kurosawa, M. K. (2008b) Friction drive of an SAW motor. Part II: Analyses, *IEEE Transactions on Ultrasonics, Ferroelectrics, and Frequency Control*, Vol. 55, 2016-2024.

Shigematsu, T. & Kurosawa, M. K. (2008c) Friction drive of an SAW motor. Part III: Modeling, *IEEE Transactions on Ultrasonics, Ferroelectrics, and Frequency Control*, Vol.55, 2066-2276.

Shigematsu, T. & Kurosawa, M. K. (2008d) Friction drive of an SAW motor. Part IV: Physics of contact, *IEEE Transactions on Ultrasonics, Ferroelectrics, and Frequency Control*, Vol.55, 2277-2287.

Shigematsu, T. & Kurosawa, M. K. (2008e) Friction drive of an SAW motor. Part V: Design criteria, *IEEE Transactions on Ultrasonics, Ferroelectrics, and Frequency Control*, Vol.55, 2288-2297.

Shiokawa, S., Matsui, Y. & Ueda, T. (1989) Liquid streaming and droplet formation caused by leaky Rayleigh waves, *IEEE Ultrasonic Symposium Proceedings*, 643-646.

Shiokawa, S., Matsui, Y. & Ueda, T. (1990) Study on SAW streaming and its application to fluid devices, *Japanese Journal of Applied Physics*, Vol. 29, 137-139.

Shiokawa, S. & Matsui, Y. (1995) The dynamics of SAW streaming and its application to fluid devices, *Material research Society Symposium Proceeding*, Vol. 360, 53-64

Takasaki, M., Osakabe, N., Kurosawa, M. & Higuchi T. (1998) Miniaturization of surface acoustic wave linear motor, *IEEE Ultrasonic Symposium Proceedings*, 679-682.

Takasaki, M., Kurosawa, M. K. & Higuchi T., (2000) Optimum contact conditions for miniaturized of surface acoustic wave linear motor, *Ultrasonics*, Vol. 38, 51-53.

Takeuchi, M., Abe, H. and Yamanouchi, K. (1994) Ultrasonic micromanipulation of small particles in liquid using VHF-range keaky wave transducer, *IEEE Ultrasonic Symposium Proceedings*, 607-610.

Takeuchi, M. and Nakano, K. (2005) Ultrasonic micromanipulation of liquid droplets for a lab-on-a-chip, *IEEE Ultrasonic Symposium Proceedings*, 1518-1521.

Timoshenko, S. & Goodier, J. (1970) *Theory of Elasticity*, Third Edition, McGraw-Hill, New York, USA.

Uchida, T.; Suzuki, T. & Shiokawa, S. (1995) Investigation of acoustic streaming excited by surface acoustic waves, *IEEE Ultrasonic Symposium Proceedings*, 1081-1084.

Ueha, S. & Tomikawa, Y. (1993) *Ultrasonic Motors: Theory and Application*, Oxford Science Publication, London, UK

Viktorov, I. A. (1967) *Rayleigh and Lamb Waves*, Plenum, New York, USA.

White, R. M. (1970) Surface elastic waves, *Proceedings IEEE Micro-electro-mechanical Systems*, Vol. 58, 1238-1276.

Yamayoshi, Y. & Hirose, S. (1992) Ultrasonic motor not using mechanical friction force, *International Journal of Applied Electro-magnetics in Materials*, Vol. 3, 179-182.

Yeo, L. Y. & Friend, J. R. (2009) Ultrafast microfluidics using surface acoustic waves, *Biomicrofluidics*, Vol. 3, 012002.

Zhang, G. M.; Cheng, L. P.; Zhang, S. Y.; Yu, J. & Shui, X. J. (2000) Surface acoustics wave rotation motor, *Electronics Letters*, Vol. 36, 1437-1438.

Zhang, H.; Dong, S. X.; Zhang, S. Y.; Wang, T. H.; Zhang, Z. N. & Fan, L. (2006) Ultrasonic micro-motor using miniature piezoelectric tube with diameter of 1.0 mm, *Ultrasonics*, Vol. 44, e603-e606.

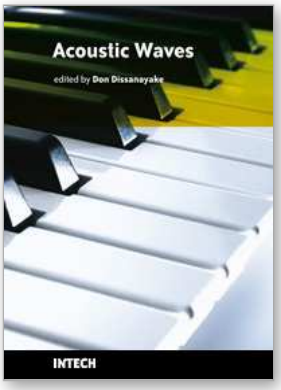

Acoustic Waves

Edited by Don Dissanayake

ISBN 978-953-307-111-4
Hard cover, 434 pages
Publisher Sciyo
Published online 28, September, 2010
Published in print edition September, 2010

SAW devices are widely used in multitude of device concepts mainly in MEMS and communication electronics. As such, SAW based micro sensors, actuators and communication electronic devices are well known applications of SAW technology. For example, SAW based passive micro sensors are capable of measuring physical properties such as temperature, pressure, variation in chemical properties, and SAW based communication devices perform a range of signal processing functions, such as delay lines, filters, resonators, pulse compressors, and convolvers. In recent decades, SAW based low-powered actuators and microfluidic devices have significantly added a new dimension to SAW technology. This book consists of 20 exciting chapters composed by researchers and engineers active in the field of SAW technology, biomedical and other related engineering disciplines. The topics range from basic SAW theory, materials and phenomena to advanced applications such as sensors actuators, and communication systems. As such, in addition to theoretical analysis and numerical modelling such as Finite Element Modelling (FEM) and Finite Difference Methods (FDM) of SAW devices, SAW based actuators and micro motors, and SAW based micro sensors are some of the exciting applications presented in this book. This collection of up-to-date information and research outcomes on SAW technology will be of great interest, not only to all those working in SAW based technology, but also to many more who stand to benefit from an insight into the rich opportunities that this technology has to offer, especially to develop advanced, low-powered biomedical implants and passive communication devices.

How to reference

In order to correctly reference this scholarly work, feel free to copy and paste the following:

Shu-yi Zhang and Li-ping Cheng (2010). Surface Acoustic Wave Motors and Actuators: Structure, Mechanism, Characteristic and Application, Acoustic Waves, Don Dissanayake (Ed.), ISBN: 978-953-307-111-4, InTech, Available from: http://www.intechopen.com/books/acoustic-waves/surface-acoustic-wave-motors-and-actuators-structure-mechanism-characteristic-and-application

INTECH
open science | open minds

InTech Europe
University Campus STeP Ri
Slavka Krautzeka 83/A
51000 Rijeka, Croatia

InTech China
Unit 405, Office Block, Hotel Equatorial Shanghai
No.65, Yan An Road (West), Shanghai, 200040, China
中国上海市延安西路65号上海国际贵都大饭店办公楼405单元

Phone: +385 (51) 770 447
Fax: +385 (51) 686 166
www.intechopen.com

Phone: +86-21-62489820
Fax: +86-21-62489821